01 Jan 1988

Electron Loss From Helium Atoms By Collisions With Fully Stripped Ions

A. E. Wetmore

Ronald E. Olson
Missouri University of Science and Technology, olson@mst.edu

Recommended Citation

A. E. Wetmore and R. E. Olson, "Electron Loss From Helium Atoms By Collisions With Fully Stripped Ions," *Physical Review A*, vol. 38, no. 11, pp. 5563 - 5570, American Physical Society, Jan 1988.
The definitive version is available at https://doi.org/10.1103/PhysRevA.38.5563

Electron loss from helium atoms by collisions with fully stripped ions

A. E. Wetmore and R. E. Olson
Department of Physics and Laboratory for Atomic and Molecular Research, University of Missouri–Rolla, Rolla, Missouri 65401-0249
(Received 27 June 1988)

Electron-loss cross sections have been calculated for fully stripped ions with charge states +1 to +100 colliding with helium atoms in the energy range 100–1000 kev/amu. The classical-trajectory Monte Carlo method was used along with a model of the helium atom with two active electrons. The reactions studied were single and double ionization, single- and double-electron capture, and electron capture plus ionization. Cross sections for the single-electron-removal reactions agree well with experimental data. Double-electron-removal cross sections are in qualitative agreement with experimental results. The n-level distributions following electron capture show that the electron-capture–plus–ionization and double–electron-capture processes are peaked at a lower n level relative to single-electron capture.

INTRODUCTION

One of the major problems in a quantum-mechanical treatment of electron loss from multielectron atoms is how to treat the dissimilar processes of ionization and charge transfer when they both contribute significantly to the cross section. In this paper we describe one method of applying the classical-trajectory Monte Carlo (CTMC) method to electron loss from helium atoms caused by collisions with intermediate-energy (100–1000 keV/amu) fully stripped ions.

Conceptually the helium atom is the simplest two-electron atomic system and is also an excellent target for experimental work. Similarly, bare nuclei have no electronic structure prior to the collision and are the simplest particles which will induce electron capture or ionization.

The collision processes that were studied include

$$A^{q+}+\mathrm{He}\rightarrow A^{q+}+\mathrm{He} \tag{1a}$$

$$\rightarrow A^{q+}+\mathrm{He}^{1+}+e^{-} \tag{1b}$$

$$\rightarrow A^{q+}+\mathrm{He}^{2+}+2e^{-} \tag{1c}$$

$$\rightarrow A^{(q-1)+}+\mathrm{He}^{1+} \tag{1d}$$

$$\rightarrow A^{(q-2)+}+\mathrm{He}^{2+} \tag{1e}$$

$$\rightarrow A^{(q-2)+}+\mathrm{He}^{1+}+e^{-}\ , \tag{1f}$$

where the ion A^{q+} is a fully stripped atomic ion. The identification of the inelastic channels is (1b), single ionization; (1c), double ionization; (1d), single-electron capture; (1e), double electron capture; and (1f), electron capture plus ionization.

The classical-trajectory Monte Carlo (CTMC) method treats the particles in the collision projectile, target nucleus, and two-target electrons as classical point particles which interact through Coulomb's law with their motion as governed by Newton's laws. The CTMC method as it applies to three-body collisions has been discussed by Percival and Richards.[1] The major difference between the four-body CTMC method and the three-body method is that our target atom with two-target electrons is not stable against small perturbations if all interparticle forces are included. The resulting autoionization is a nonphysical result which is not encountered in quantum-mechanical theories.

Several modifications to the standard CTMC method to avoid the autoionization problem have been examined in the past. The first was the independent-electron model[2,3] which expresses multielectron cross sections as combinations of probabilities from single-electron atoms. Recent work by Peach *et al.*[4] and Willis *et al.*[5] has expanded upon the independent-electron model by replacing the Coulomb interaction in the CTMC method with an appropriate model potential. In a more direct attack the CTMC method was applied to fast collisions (1–5 MeV/amu) where the target does not have time to autoionize before the collision is completed.[6,7] While this method proved to yield useful information, it completely precludes obtaining cross sections from an important range of energies, $E<500$ keV/amu. Another method[8,9] was the use of a non-Coulomb restoring force which was added to the interactions to prevent either electron from collapsing into the nucleus and so prevent autoionization.

The restoring force is added to the Hamiltonian as a velocity-dependent repulsive force centered at the nucleus. This force simulates the quantum mechanics by keeping the electron from collapsing into the nucleus. The form of the Hamiltonian used for the helium atom is

$$\mathcal{H}=\sum_{k=1}^{4}\frac{p_k^2}{2m_k}+\sum_{k=1}^{3}\sum_{j=k+1}^{4}\frac{q_kq_j}{r_{kj}}+\sum_{i=1}^{2}V(r_i,p_i)\ , \tag{2}$$

where

$$V(r_i,p_i)=\left[\frac{\xi^2}{4\alpha r_i^2}\right]\exp\left\{\alpha\left[1-\left[\frac{r_ip_i}{\xi}\right]^4\right]\right\}. \tag{3}$$

The calculations[9] using restoring forces did not attempt to treat the double-electron capture reaction, (1e).

The present work examines the electron-loss process within the classical-trajectory Monte Carlo framework from a modified Hartree-Fock perspective. Our model of the helium atom removes the electron-electron force and allows each electron to interact with the target nucleus through a separate Coulomb potential. The Coulomb potentials are assigned by adding electrons in Bohr orbits to a bare nucleus one by one with the experimentally observed ionization energies.

The remainder of this paper is divided into five sections: (1) the spatial and momentum distributions of the simulated helium-atom target; (2) the high-energy limit; (3) total cross sections; (4) n-level distributions of electron-capture cross sections; and (5) conclusions.

INITIAL ELECTRON DISTRIBUTIONS

When using the CTMC method a primary consideration is that the ensemble of initial states of the target atom closely mimics the actual momentum distribution of the target electrons.[1] The spatial distribution of the electrons, the angular momenta distributions, and correlations between the electrons are also of interest. We have attempted to model the momentum distribution with the most fidelity, then adjusted the angular momentum distribution to obtain the electron-electron correlations.

For the helium atom we are fortunate to have an extremely accurate tabulation of the electron momentum distribution from the work of Regier and Thakkar.[10] For the CTMC model we sum the contribution from the two electrons, each of which is of the form

$$\rho(p)=\frac{8p_n^5}{\pi^2(p^2+p_n^2)^4} \tag{4}$$

for Bohr orbits with a microcanonical distribution of angular momenta.[1] In Eq. (4) the p_n is the momentum associated with a binding energy of E_n. Choosing the binding energies to reflect the proper total energy and ionization energies yields the result

$$\rho(p)=\frac{8(2mE_1)^{5/2}}{\pi^2(p^2+2mE_1)^4}+\frac{8(2mE_2)^{5/2}}{\pi^2(p^2+2mE_2)^4}\ , \tag{5}$$

with the energies E_1 and E_2 being 2.0 and 0.904 a.u.

The result from Eq. (5) is compared in Fig. 1 with the results tabulated by Regier and Thakkar.[10] Also included for comparison is the momentum distribution for two electrons in identical Bohr orbits with the proper total energy. It can be seen in Fig. 1 that by using the individual binding energies to define the Bohr orbits for the two electrons, the momentum distribution is greatly improved at small momentum values. The agreement is also slightly better for large values of the momentum. Because of this we have chosen to use the "split-shell" model where one electron is bound by the first ionization potential and the other electron is bound by the second ionization potential.[11] This automatically ensures that the helium atom target will have the proper total energy and that there will not be the drawback of having an unphysical first and second ionization potential.

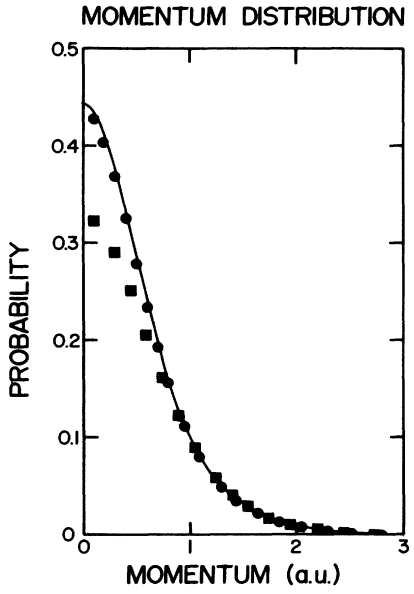

FIG. 1. Momentum distribution for the helium atom. The line is the quantum-mechanical result of Regier and Thakkar (Ref. 10). The Monte Carlo results are for ■, identical electrons and ●, split-shell model.

We are fortunate that these choices of the binding energies replicate the momentum distribution of the helium atom so well. It is because the classical and quantal differential scattering cross sections for particles interacting through a Coulomb potential are identical functions of the relative velocity (momentum) that the CTMC method works. Without the agreement between the momentum distributions our use of the CTMC method would be inappropriate.

As is known from work on three-body CTMC calculations, the radial distribution of the classical Bohr orbit does not agree with the quantum-mechanical results.[1,11] In particular, the classical model has a maximum value for the allowed separation between the target nucleus and the bound electron. Beyond this distance is the classically forbidden region. The general success of the three-body Monte Carlo calculations has shown that the sharp cutoff in the radial distribution is not a serious drawback. Efforts to improve the radial distribution[11] while somewhat successful have not been pursued.

The radial probability density for a single electron in a classical Bohr orbit is given by[11]

$$\rho(r)=\frac{16}{\pi R_i^3}r^2\left[\frac{R_i}{r}-1\right]^{1/2}\ , \tag{6}$$

with

$$R_i=\frac{Z_j}{E_i}\ , \tag{7}$$

where Z_j is the effective nucleus charge seen by the orbiting electron. For two electrons with binding energies E_1 and E_2 and effective charges Z_1 and Z_2 this becomes

$$\rho(r)=\frac{16}{\pi R_1^3}r^2\left[\frac{R_1}{r}-1\right]^{1/2}+\frac{16}{\pi R_2^3}r^2\left[\frac{R_2}{r}-1\right]^{1/2} . \quad (8)$$

The square roots in Eq. (8) are replaced by zero for negative arguments. Figure 2 shows a comparison of the radial probability density as described by Eq. (8) for electrons with binding energies of 2.0 and 0.904 a.u., i.e., effective nuclear charges of 2.000 and 1.344. As in the plot of momentum distributions the case of two identical electrons is also shown along with the quantum-mechanical results of Regier and Thakkar.[10]

The angular momentum distribution of the electrons is treated somewhat differently than in the three-body Monte Carlo method. In that case the angular momentum of the electron is allowed to span the range from 0 to 1. However, just as the single electron's angular momentum represents an s state by ranging from 0 to 1, the total angular momentum of the two electrons represents an S state by having the total angular momentum distributed uniformly between 0 and 1. This is similar to the method chosen by Peach *et al.*[4] to represent an arbitrary L state in their CTMC calculations. Unfortunately the total angular momentum, L is a function of the two individual angular momenta (l_1,l_2) and the angle (θ_{12}) between the planes of the Bohr Orbits.

$$L^2=l_1^2+l_2^2+2l_1l_2\cos(\theta_{12}) . \quad (9)$$

To make the distribution of the total angular momentum closer to the desired uniform distribution we modified the way in which the target electrons are initialized. The original method of choosing the individual angular momenta and angle between the planes of the Bohr orbits closely followed the method used in the three-body CTMC method. The model of Coveny and Child[12] has a fixed angle of 120° between the planes of the electron orbits and a fixed eccentricity of 0.866 for each of the electron orbits. We modified the angular momentum for each electron by selecting an eccentricity for the Bohr orbit in the range from 0 to 1, then set the angle between the planes of the orbits to 120°. This allowed each electron to properly sample the angular momentum distribution and limited the total angular momentum to 1. The drawback to this was that the fixed angle between the Bohr orbits precluded the two electrons from ever being completely opposite the nucleus from each other.

Therefore, to expand the range of orientations available to the electrons we developed a method of initialization by choosing the angle between the planes of the Bohr orbits so that the cosine of one half the angle was uniformly distributed between 0 and 1. This allowed all relative orientations of the electrons and orbits. It also introduced situations where the total angular momentum was greater than 1. In the computer program we rejected any cases where the total electron angular momentum was greater than 1 and selected new random values for the individual angular momenta and angle between the planes of the Bohr orbits until we had a configuration with total angular momentum less than or equal to 1. The result of this method of choosing the initial electron coordinates was an alteration of the distribution of the individual electron angular momenta towards lower values. The angular momentum distributions for these initial conditions are shown in Fig. 3.

We also calculated the expectation values of several parameters which can be compared to quantum-mechanical values for the helium atom.[10] These are listed in Table I. The radial expectation values are somewhat smaller than the "true" values. Also, the distance between the electrons is smaller. This means that our atom is more local-

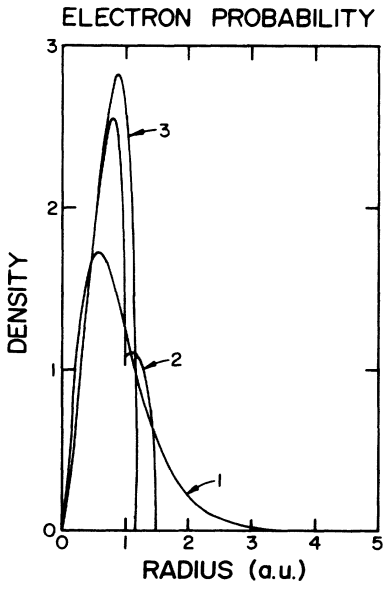

FIG. 2. Electron radial probability density for the helium atom. The identification is 1, Regier and Thakkar (Ref. 10), 2, CTMC identical electrons, and 3, CTMC split-shell model.

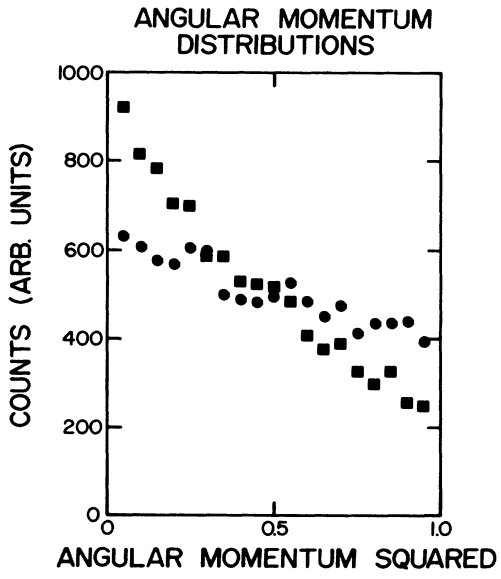

FIG. 3. Angular momentum distribution for the model helium atom. Individual electron l^2, ●; total L^2, ■.

TABLE I. Expectation values for the helium atom.

Property	Regier and Thakkar	CTMC
$\langle r \rangle$	0.929	0.789
$\langle r_{12} \rangle$	1.422	1.029
θ_{12} (deg.)	90.7	80.8
$\langle p \rangle$	2.81459	2.798
$\langle p_{12} \rangle$	2.0291	2.068

ized due to the lack of penetration to the nonclassical region. The expectation value of the angle between the electrons is greater than 80°. Taken together these mean that even without any explicit electron-electron interactions we have a significant amount of correlation between the electrons. This arises from the elliptical Bohr orbits and the restriction on the total angular momentum of the electrons. As is required by the CTMC method the momenta of the electrons are well represented by our procedure.

HIGH ENERGY

Figure 4 shows the cross sections for electron capture plus ionization, single ionization, and double ionization as a function of projectile charge at 1 MeV/amu. The Monte Carlo results are in very good agreement for all three processes over a range spanning five orders of magnitude in the cross sections and two orders of magnitude in projectile charge. The results are similar to those calculated by McKenzie and Olson[7] using a model for the helium atom with circular orbits for electrons. At energies greater than 1 MeV the collisions will be fast enough that autoionization made possible by the electron-electron Coulomb interaction will not significantly change the cross sections.

Recent measurements are now available to compare our calculations to high values of the incident ion's charge state. Two measurements are available for $q=44$. The measurement by McGuire *et al.*[13] is in good agreement with our results. The measurement of Datz *et al.*[14] is significantly lower. The single- and double-ionization cross sections of Datz *et al.*[14] have approximately the correct relative magnitude but are inconsistent with the other experiments and the CTMC calculations. For lower-charge projectiles the calculations are in good agreement with experimental data. We find that the ratio of single to double ionization decreases with increasing charge state in qualitative agreement with the experimental results of McGuire *et al.*[13] and Datz *et al.*[14] We also note the increasing importance of the electron-capture-plus-ionization cross section as a double-electron-removal process for high-charge state projectiles.

TOTAL CROSS SECTIONS

Figure 5 shows the total cross sections for single ionization as a function of energy for fully stripped ions colliding with helium atoms. To allow combining the vari-

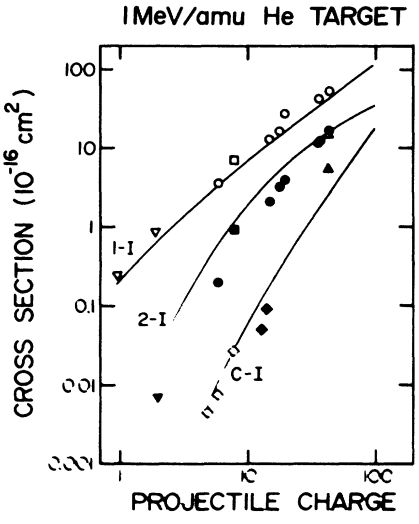

FIG. 4. Total cross sections at 1 MeV/amu energy. Single ionization, 1-I; double ionization, 2-I; and electron capture, C-I. Experimental results for single ionization: Datz *et al.* (Ref. 14), △; Shah and Gilbody (Ref. 15), ▽; Hvelplund *et al.* (Ref. 21), □; McGuire *et al.* (Ref. 13), ○. Experimental results for double ionization: Datz *et al.* (Ref. 18), ▲; Shah and Gilbody (Ref. 15), ▽; Hvelplund *et al.* (Ref. 21), ■; McGuire *et al.* (Ref. 13), ●. Experimental results for electron capture plus ionization: Guffey *et al.* (Ref. 16), ◇; Schiebel *et al.* (Ref. 22), ◆.

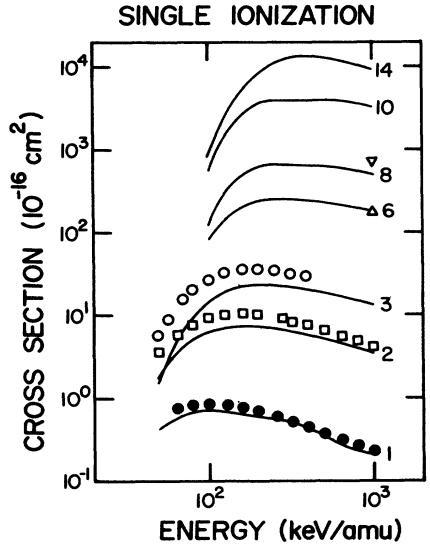

FIG. 5. Single-ionization cross sections. The lines 1, 2, 3, 6, 8, 10, and 14 are the CTMC calculations of the following: H^+, 1; $\times 5\,He^{2+}$, 2; $\times 10\,Li^{3+}$, 3; $\times 50$ C^{6+}, 6; $\times 100$ O^{8+}, 8; $\times 500\,Ne^{10+}$, 10; $\times 1000\,Si^{14+}$, 14. The markers are the experimental data for H^+, ○; He^{2+}, □; and Li^{3+}, ●; of Shah and Gilbody (Ref. 15). Also included are the measurements of McGuire *et al.* (Ref. 13) for C^{6+}, △; and Hvelplund *et al.* (Ref. 21) for O^{8+}, ▽.

ous cross sections on a single plot Figs. 5–9 have a scaling factor applied to the various charge states. The CTMC calculations include two components which are combined to obtain the results which are shown. The first component is the reaction [Eq. (1b)], single ionization. The second component is the formation of excited states with sufficient energy for one of the electrons to ionize.

$$A^{q+}+\mathrm{He}\rightarrow A^{q+}+\mathrm{He}^{**}\rightarrow A^{q+}+\mathrm{He}^{+}+e^{-} . \quad (10)$$

We examined the trajectories leading to reaction 1*a* and calculated the total internal energy transferred to the target by the projectile. If the target has absorbed more energy than the first ionization potential we treat the collisions as a "virtual ionization" event. Because of the nature of the split shell model for the target electrons, ionization of the tightly bound electron is much less likely than ionization of the weakly bound electron. The agreement with experiment[15] when we add the "virtual loss" events suggests that the controlling factor for the ionization cross section is the energy deposited to the target. For low charge state projectiles the impact-parameter range which produces ionization is about the size of the target atom. The classical radial limit of the electron orbits reduces the energy that larger impact-parameter collisions can transfer to the target electrons. This would tend to make the CTMC calculation underestimate the single-ionization cross section. For projectiles with large q the interaction is of such long range that the size of the target is a much less important factor. Such is the behavior we find.

Figure 6 shows the cross sections for single-electron capture [(Eq. (1c)]. The results for H^+, He^{2+}, and Li^{3+} are in excellent agreement with the experimental data of Shah and Gilbody.[15] The K-shell x-ray cross sections of Guffey *et al.*[16] are somewhat larger than our results in the energy range 250–500 keV. Since the measurements were not a coincidence-type experiment, they do not separate the electron-capture [Eq. (1d)] and electron-capture–plus–ionization [Eq. (1f)] channels. These two channels are of about the same magnitude at these energies; combination of these two channels in the experiment would tend to overestimate either of the two individual cross sections. Previous CTMC studies have observed that the velocity matching between the projectile and the target electron is very important in electron-capture reactions.[17] We attribute the excellent agreement of the electron-capture cross section to the quality of the split-shell model momentum distribution.

Electron-capture–plus–ionization cross sections are shown in Fig. 7. In addition to the direct electron-capture plus ionization that we calculate, the measurements of Datz and co-workers[14,18] show that autoionizing double capture can be an important route to electron capture plus ionization. The double-electron capture which we have calculated is often into doubly excited states that will decay through the Auger process. Only when the interval between available energy levels is greater than 10 keV will radiative decay predominate.[19] As part of the final-state analysis in the CTMC program we examine the binding energy of each electron which undergoes electron capture. From this energy and our knowledge of the one-electron ground-state energy we assigned a principal quantum number n. If both electrons are in excited states, the reaction is flagged as autoionizing double-electron capture. On Fig. 7 the sum of the direct electron capture plus ionization, Eq. (1f), and the autoionizing

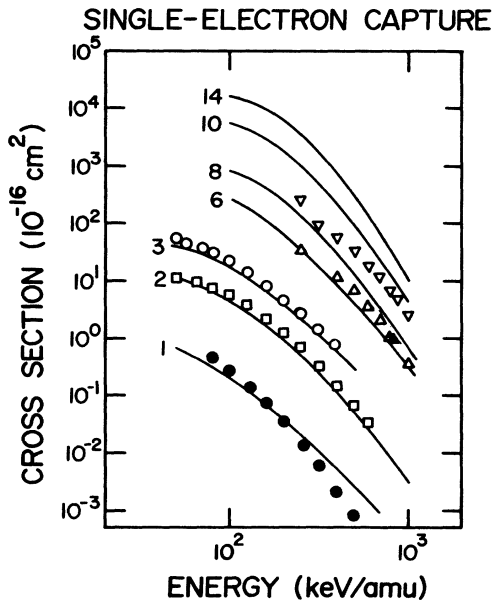

FIG. 6. Single-electron-capture cross sections. The identification and the scaling factors for the CTMC results and the experimental data of Shah and Gilbody (Ref. 15) are the same as in Fig. 5. Also shown are the results of Guffey *et al.* (Ref. 16) for O^{6+}, △; and O^{8+}, ▽.

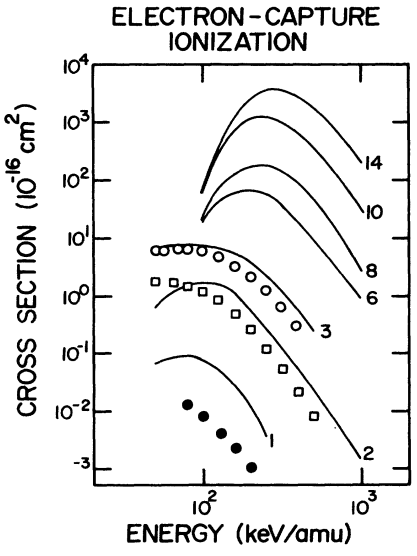

FIG. 7. Electron-capture–plus–ionization cross sections. The contribution from autoionizing double-electron capture is included in this cross section. The identification and the scaling factors for the CTMC results and the experimental data of Shah and Gilbody (Ref. 15) are the same as in Fig. 5.

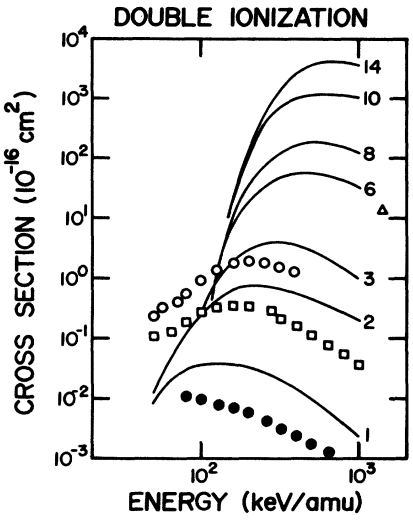

FIG. 8. Double-ionization cross sections. The identification and the scaling factors for the CTMC results and the experimental data of Shah and Gilbody (Ref. 15) are the same as in Fig. 5. Also shown is the experimental datum of McGuire *et al.* (Ref. 13) for C^{6+} at 1.4 MeV/amu, △.

portion of the double-electron capture, Eq. (1e), is shown.

Double-ionization cross sections are shown in Fig. 8. The CTMC calculations are significantly above the experimental data of Shah and Gilbody.[15] The trend from H^+ to Li^{3+} is one of improving agreement with the experiment. The effect of the radial electron distribution is different in the case of double ionization. Since only small impact-parameter collisions will lead to double ionization the peak in the radial electron probability shown in Fig. 2 will tend to cause the CTMC calculation to overestimate the double-ionization cross sections. The correlation between the electrons such as both being on the same side of the nucleus as the projectile during the collision will be an important factor in allowing this reaction to occur.

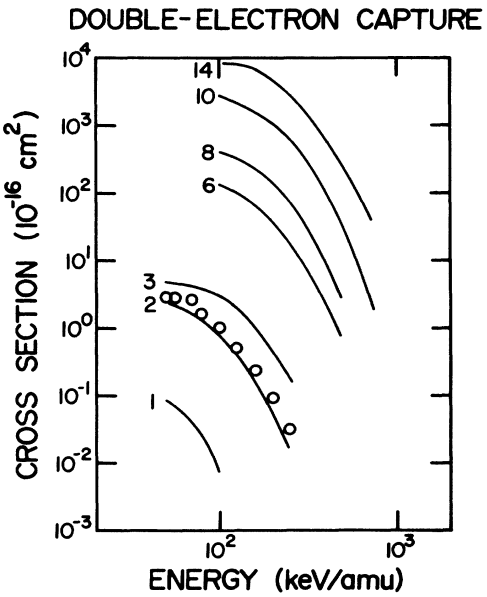

FIG. 9. Double-electron-capture cross sections. The autoionizing double-electron capture is not included in these cross sections. The identification and the scaling factors for the CTMC calculations are the same as in Fig. 5. The data of Shah and Gilbody (Ref. 15) for Li^{3+}, ○, is also shown.

The double-electron-capture cross sections are shown in Fig. 9. The data is in qualitative agreement with the results of Shah and Gilbody.[15] While the energy dependence of the single-electron-capture and double-electron-capture cross sections suggests that a similar process could be taking place, our analysis of the n-level distributions of the final state of the captured electrons described in the next section suggest otherwise. If there are different mechanisms responsible for these reactions then results obtained by using the independent-electron approximation should not be an adequate description.

N-LEVEL DISTRIBUTIONS OF CHARGE-EXCHANGE ELECTRONS

Recent experiments[14] have suggested that simple charge-exchange electrons [Eq. (1d)] are captured into n levels with a distribution which has a peak at a larger value of n than electrons from the electron-capture–plus–ionization process [Eq. (1f)]. The existence of a peak in the n-level distribution for electron capture from hydrogenic targets has been described by Olson.[20] The location of the peak has been attributed to the attempt to maintain both the electron's orbital energy,

$$E=\frac{\varepsilon}{n^2}\ , \tag{11}$$

and the dimension of its orbit,

$$\langle r\rangle\approx\frac{n^2}{\sqrt{2\varepsilon}}\ , \tag{12}$$

where ε is the ground-state energy of the electron. Since the energy relation would require that

$$n_f=n_i\left[\frac{\varepsilon_f}{\varepsilon_i}\right]^{1/2} \tag{13}$$

at resonance and the orbital size criteria requires that

$$n_f=n_i\left|\frac{\varepsilon_f}{\varepsilon_i}\right|^{1/4} \tag{14}$$

it is impossible to satisfy both at once. The earlier CTMC calculations[20] showed that the n level with the largest contribution, n_{peak}, was given by

$$n_{\text{peak}}\approx n_i\left[\frac{\varepsilon_f}{\varepsilon_i}\right]^{3/8}\ . \tag{15}$$

The preliminary results of Datz *et al.*[14] for 15-times-ionized projectiles colliding with He atoms at 100 keV/amu find the cross section for electron capture into

the $n=6$ level is about half as large for electron capture plus ionization as it is for direct electron capture. For capture into the $n=10$ level the ratio is 0.1. These measurements were made by observing the vuv photons from the $n=6$ to 5 and $n=10$ to 9 transitions in coincidence with the He^+ and He^{2+} ions. The interpretation of these results is that the electron-capture–plus–ionization cross section is peaked at a smaller n level than the single-electron-capture cross section. Figure 10 shows the results from the CTMC calculation for single- and double-electron capture at 100 keV/amu for P^{15+} on He. Also included are the relative data of Datz *et al.*[18] normalized to our absolute single-electron-capture cross section. At this energy we find no direct electron capture plus ionization. The double-electron capture is primarily to the $n=4$ and 5 levels. These levels will stabilize through the Auger process yielding electron capture plus ionization. This will tend to shift the final n level to even lower values.

When we examine the final-state n levels at 250 keV/amu for all electrons undergoing electron capture, Fig. 11, we see all three electron capture processes [Eqs. (1d), (1e), and (1f)] occurring. The nature of the n-level distributions yields some interesting insights into the mechanisms involved in the electron-capture processes. In Fig. 11 we have plotted the relative size of the cross sections for the various electron-capture processes as a function of final-state n level of the captured electron. For double-electron capture the n levels are calculated using a hydrogenic model with no screening. Each of the curves has been normalized to the size of the n level with the largest cross section. Examining Fig. 11 we see that the distribution of n levels for single-electron capture is

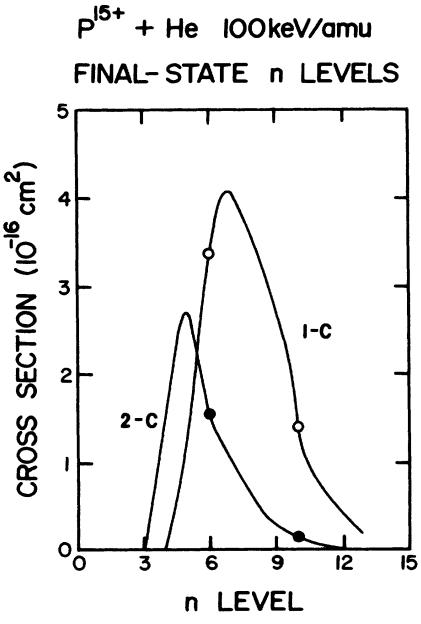

FIG. 10. P^{15+} n levels. 1-C, single-electron capture; 2-C, double-electron capture. The circles are the data of Datz *et al.* (Ref. 18). The collision energy is 100 kev/amu.

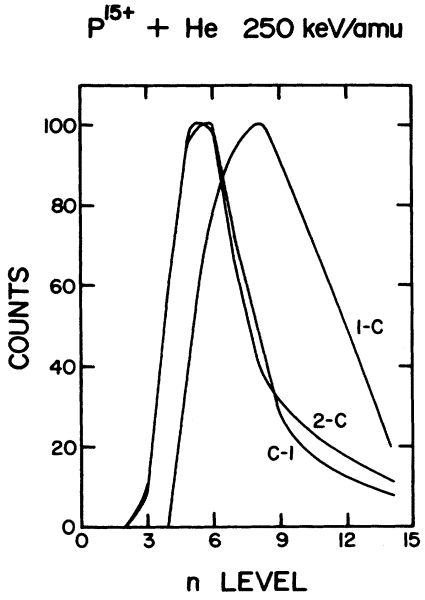

FIG. 11. P^{15+} n levels. 1-C, single-electron capture; 2-C, double-electron capture; C-I electron capture plus ionization. The collision energy is 250 keV/amu.

much broader than those for the two-electron processes of double-electron capture or electron capture plus ionization. This suggests that the mechanism for both of the two-electron-removal processes is similar and in some sense fundamentally different from the one-electron-removal process.

The similarity of the double-electron capture and electron-capture–plus–ionization n-level distributions suggests that both proceed through a similar intermediate state which evolves into the separate final states. The difference in the n-level distribution of the single-electron-capture cross section suggests that such a route is not followed.

If the two-electron processes take place by a mechanism different from the single-electron-capture process it implies that other theoretical approaches may have to be modified. The independent-electron approximation would be inappropriate if cooperative mechanisms are involved. For quantum-mechanical methods it suggests that multicenter methods could be appropriate and that including continuum states would be very important.

CONCLUSIONS

We have developed a general four-body version of the classical-trajectory Monte Carlo method and a model for helium-atom targets with nonequivalent electrons. The excellent agreement for single-electron-capture cross sections is attributed to the very accurate momentum distribution of the split-shell model. The single-ionization and double-ionization cross sections suggest that the radial electron distribution limits the ability of the CTMC method to model the energy deposition leading to ionization. The agreement with experimental data suggests a

range of validity from 100 to 1 MeV/amu for all fully stripped atomic projectiles colliding with helium. In addition, the n-level distributions of the electron-capture processes suggests that the two-electron processes of electron capture plus ionization and double-electron capture proceed through a different mechanism from the single-electron-capture process; this implies that quantum-mechanical calculations of the double-electron processes should include continuum states and could benefit from multicentered techniques.

ACKNOWLEDGMENT

This work was supported by the Office of Fusion Research of the U.S. Department of Energy.

[1]I. C. Percival and D. Richards, Adv. At. Mol. Phys. **11**, 1 (1975).
[2]R. E. Olson, Phys. Rev. A **18**, 2464 (1978).
[3]R. E. Olson, J. Phys. B **12**, 1843 (1979).
[4]G. Peach, S. L. Willis, and M. R. C. McDowell, J. Phys. B **18**, 3921 (1985).
[5]S. L. Willis, G. Peach, M. R. C. McDowell, and J. Banerji, J. Phys. B **18**, 3939 (1985).
[6]S. J. Pfeifer and R. E. Olson, Phys. Lett. **92A**, 175 (1982).
[7]M. L. McKenzie and R. E. Olson, Phys. Rev. A **35**, 2863 (1987).
[8]C. L. Kirschbaum and L. Wilets, Phys. Rev. A **21**, 834 (1980).
[9]D. Zajfman and D. Maor, Phys. Rev. Lett. **56**, 320 (1986).
[10]P. E. Regier and A. J. Thakkar, J. Phys. B **18**, 3061 (1985).
[11]D. J. W. Hardie and R. E. Olson, J. Phys. B **16**, 1983 (1983).
[12]P. V. Coveny and M. S. Child, J. Phys. B **17**, 319 (1984).
[13]J. H. McGuire, A. Muller, B. Schuch, W. Groh, and E. Salzborn, Phys. Rev. A **35**, 2479 (1987).
[14]S. Datz, R. Hippler. L. H. Andersen, P. F. Dittner, H. Knudsen, H. F. Krause, P. D. Miller, P. L. Pepmiller, T. Rosseel, N. Stolterfelt, Y. Yamazaki, and C. R. Vane, Nucl. Instrum. Methods, Phys. Res. **A62**, 62 (1987).
[15]M. B. Shah and H. B. Gilbody, J. Phys. B **18**, 899 (1985).
[16]J. A. Guffey, L. D. Ellsworth, and J. R. Macdonald, Phys. Rev. A **15**, 1863 (1977).
[17]R. Abrines and I. C. Percival, Proc. Phys. Soc. London, **88**, 873 (1966).
[18]S. Datz, C. Bottcher, L. H. Andersen, P. Hvelplund, and H. Knudsen, Nucl. Instrum. Methods Phys. Res. **10**, 116 (1985).
[19]T. A. Carlson, Radiat. Res. **64**, 53 (1975).
[20]R. E. Olson, Phys. Rev. A **24**, 1726 (1981).
[21]P. Hvelplund, H. K. Haugen, and H. Knudsen, Phys. Rev. A **22**, 1930 (1980).
[22]U. Schiebel, B. L. Doyle, J. R. Macdonald, and L. D. Ellsworth, Phys. Rev. A **16**, 1089 (1977).